Deconvolution of the electronic density of states of tip and sample from scanning tunneling spectroscopy data: Proof of principle

B. Koslowski, H. Pfeifer, and P. Ziemann
Institut für Festkörperphysik, Universität Ulm, D-89069 Ulm, Germany
(Received 28 April 2009; revised manuscript received 24 July 2009; published 20 October 2009)

It is demonstrated that deconvolution of the density of states (DOS) of tip and sample from scanning tunneling spectroscopy data is possible within the framework of a one-dimensional Wentzel-Kramers-Brillouin approximation if additional information such as data sets taken at two sufficiently different tip-sample separations is provided. The basic concept is to convert the underlying integral equation for the tunneling current by differentiation with respect to the sample bias (first set) and, in addition, with respect to the tip-sample separation (second set) into two sets of Volterra integral equations of the second kind with two equations for the tip and another two for the sample DOS. Though these integro-differential equations can in principle be solved numerically employing the Neumann approximation scheme, it turns out in practice that suitable iteration schemes have to be found to guarantee stable solutions. Employing tunneling data taken at two sufficiently different tip-sample separations, it is demonstrated that iterating suitably through the system of equations results in a recovery and deconvolution of the tip and sample DOS. The underlying formalism is derived, examples are given and limitations discussed. Finally, we apply an adapted procedure to experimental data obtained on Nb(110) and compare the deconvolved sample DOS with density-functional theory data.

DOI: 10.1103/PhysRevB.80.165419 PACS number(s): 68.37.Ef, 73.40.Gk

I. INTRODUCTION

Ever since the first experiments on electrons tunneling through a barrier between two metals and their description in terms of a one-dimensional (1D) Wentzel-Kramers-Brillouin (WKB) approximation, one of the basic assumptions has been that the 'density of electronic states' of both metallic electrodes in this seemingly symmetric arrangement equally contribute to the total tunneling current.[1–3] Due to this symmetry, over the years the general judgment emerged that tunneling data such as current-voltage (*I*-*V*) characteristics are insufficient to extract information on DOS of both electrodes separately. The problem of arriving at such a deconvolution gets even more complicated if the transmission through the tunneling barrier is included, which generally depends strongly on the energy of the electrons. Hence, the experimentally determined tunneling current has to be described by a convolution integral over three rather than two energy-dependent functions rendering their separation impossible according to standard opinions.

The advent of scanning tunneling microscope and the accompanying development of scanning tunneling spectroscopy (STS) renewed interest in but also deepened the above deconvolution dilemma of how to extract the sample DOS separated from that of the tip. Convinced that there will be no direct solution, many experimentalists tried to derive a quantity from measured data, which at least would closely resemble the DOS of the sample and gradually the derivative or logarithmic derivative of the tunneling current with respect to the tunneling bias, $\partial_V I$, emerged and was accepted as delivering that information.[4–8] A more accurate analysis has been provided by very recent contributions.[9–13] All these approaches include the one-dimensional WKB approximation allowing a description of the transmission probability function, thereby enabling the removal of the influence of the tunneling barrier from the recovered "DOS," which, however, then still is a joint DOS of the electrodes.

Aiming at making STS independent of the specific sensor, the tunneling tip, a first idea of how to properly deconvolve the sample and tip DOS has been proposed in Ref. 9 and in the present contribution this idea will be modified and extended, and its feasibility will be demonstrated. As will be shown, it is the transmission probability function and its dependence on the tip-sample separation when taking tunneling *I*-*V* curves that breaks the seeming symmetry of the tunneling arrangement, allowing a self-consistent deconvolution of the sample and tip DOS.

II. DERIVATION OF THE VOLTERRA INTEGRAL EQUATIONS

The starting point of our calculation is the tunneling current, I, as given by the one-dimensional WKB approximation for a barrier characterized by an energy-dependent transmission coefficient, $T(E,V,z)$. Applying a bias, V, across the barrier causes a tunneling current, which reads[8,14] as (for an energy diagram see Fig. 1)

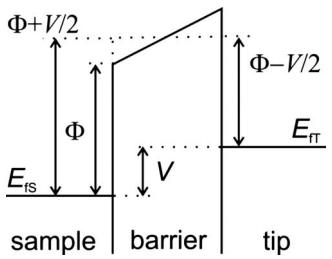

FIG. 1. Energy diagram of a tunneling junction including an applied bias. The symbols are: the Fermi energy of the sample and tip, E_{FS}, E_{FT}, respectively, the barrier height, Φ, and the applied bias, V (here in eV).

$$I(V) = \int_{-\infty}^{-\infty} \rho_S(E)\rho_T(E-V)T(E,V,z)f_{12}(E,V)dE, \quad (1)$$

where ρ_S and ρ_T are the sample and tip density of states (DOS), respectively, f_{12} is a window function $f_{12}(E,V) = f(E-V) - f(E)$ with the Fermi-Dirac distribution f, and E is the energy with respect to the Fermi energy of the sample. The area of the junction is set to unity. Though the equations derived in the following can be similarly formulated for a finite temperature, we simplify Eq. (1) for zero temperature introducing finite integral boundaries and thus resembling the appearance of a Volterra integral equation of the first kind

$$I(V) = \int_0^V \rho_S(E)\rho_T(E-V)T(E,V)dE. \quad (2)$$

According to the one-dimensional WKB approximation the transmission coefficient at zero bias is given by $T(E,z) = e^{-B\cdot\sqrt{\Phi-E}z}$ with z being the tip-sample separation, Φ being the effective tunneling barrier height, and $B = 2\sqrt{2m_e}/\hbar$ or $B=2$ for atomic units. A bias dependence of the transmission coefficient is included by the trapezoidal approximation leading to $T(E,V,z) = e^{-B\cdot\sqrt{\Phi+V/2-E}z}$. We take the derivative of Eq. (2) with respect to V resulting in

$$\partial_V I(V) = \rho_S(V)\rho_T(0)T(E=V,z) + \int_0^V \rho_S(E)T(E,V,z)\cdot\left[\partial_V\rho_T(E-V) - \frac{B\cdot z\rho_T(E-V)}{4\sqrt{\Phi+\frac{V}{2}-E}}\right]dE. \quad (3)$$

We formally solve this equation for ρ_S giving

$$\rho_S(V) = \frac{1}{\rho_T(0)T(E=V,z)}\left\{\partial_V I(V) + \int_0^V \rho_S(E)T(E,V,z) \times \left[\frac{B\cdot z\rho_T(E-V)}{4\sqrt{\Phi+\frac{V}{2}-E}} + \partial_E\rho_T(E-V)\right]dE\right\}, \quad (4)$$

where we used $-\partial_V\rho(E-V) = \partial_E\rho(E-V)$. This is a Volterra integral equation of the second kind. Such an equation can be solved numerically by the Neumann approximation scheme, where ρ_S in the integral is replaced by $\rho_{S,n}$ and ρ_S on the left side is replaced by $\rho_{S,n+1}$. To find a numerical solution of Eq. (4) one may start setting $\rho_{S,0}=0$ and assuming a reasonable $\rho_T(E)$. One immediately obtains $\rho_{S,1}(V) = \partial_V I(V)/[\rho_T(0)T(E=V,z)]$ as a first-order approximation of ρ_S. Alternatively one may start using an approximation as given in Ref. 9. Iteratively applying this scheme leads to an accurate solution in most cases even if ρ_S is not continuously differentiable. However, since we will consider a symmetric problem for both DOS numerically, both DOS should be well behaved.

An alternative to iterating the full integral equation would be to expand the kernel functions of the integrals via a Neumann series thus determining the resolvent of the integral equation. However, at this stage, we expect no advantage from the Neumann series.

The tunneling junction is symmetric and consequently we may change the reference frame from the sample to the tip interchanging the role of ρ_S and ρ_T in the formulas. This results in a Volterra integral equation for the DOS of the tip

$$\rho_T(V_T) = \frac{1}{\rho_S(V_T=0)T(E=V_T,z)} \times \left\{\partial_V I(-V_T) + \int_0^{V_T} \rho_T(E)T(E,V_T,z) \times \left[\frac{B\cdot z\rho_S(E-V_T)}{4\sqrt{\Phi+\frac{V_T}{2}-E}} + \partial_E\rho_S(E-V_T)\right]dE\right\}, \quad (5)$$

where $V_T = -V$ is the bias with respect to the tip. Note, that this equation is identical to Eq. (4) in the respective reference frame but $\partial_V I$ has been mirrored at $V=0$ because $\partial_V I$ has originally been measured in the reference frame of the sample. This is very convenient for the corresponding numerical calculations, since the same routine can be used in both cases by just interchanging the role of ρ_S and ρ_T and taking the mirror image of $\partial_V I$.

Equations (4) and (5) have already been derived earlier[9] and form the first set of Volterra integral equations. In order to derive a second set, we take the derivative of Eq. (3) with respect to the tip-sample separation, z,

$$\partial_z\partial_V I(V) = -B\sqrt{\Phi-\frac{V}{2}}\cdot\rho_S(V)\rho_T(0)T(E=V,z) + \frac{B^2}{4}zI + B\cdot\int_0^V \rho_S(E)T(E,V,z)\left[-\frac{\rho_T(E-V)}{4\sqrt{\Phi+\frac{V}{2}-E}} + \sqrt{\Phi+\frac{V}{2}-E}\cdot\partial_E\rho_T(E-V)\right]dE, \quad (6)$$

and follow the same arguments as before to obtain new Volterra integral equations

$$\rho_S(V) = \frac{1}{\rho_T(0)\sqrt{\Phi-\frac{V}{2}}T(E=V,z)}\cdot\left\{\frac{B}{4}zI(V) - \frac{\partial_z\partial_V I(V)}{B} + \int_0^V \rho_S(E)T(E,V,z)\left[-\frac{\rho_T(E-V)}{4\sqrt{\Phi+\frac{V}{2}-E}} + \sqrt{\Phi+\frac{V}{2}-E}\cdot\partial_E\rho_T(E-V)\right]dE\right\}, \quad (7)$$

and

$$\rho_T(V_T) = \frac{1}{\rho_S(0)\sqrt{\Phi - \frac{V_T}{2}}T(E=V_T,z)} \cdot \left\{ \frac{B}{4} z I(V_T) - \frac{\partial_z \partial_V I(V_T)}{B} + \int_0^{V_T} \rho_T(E) T(E,V_T,z) \left[- \frac{\rho_S(E-V_T)}{4\sqrt{\Phi + \frac{V_T}{2} - E}} + \sqrt{\Phi + \frac{V_T}{2} - E}\,\partial_E \rho_S(E-V_T) \right] dE \right\}, \quad (8)$$

where we replaced an integral by $I(V)$ and $I(V_T)$, respectively, according to Eq. (2). This shall indicate that when applying these equations to the measured tunneling characteristics, the corresponding terms may be replaced by the experimental data. Experimentally, $\partial_z \partial_V I$ may be determined by a double modulation technique using two lock-in amplifiers, by taking $\partial_V I$-z curves for a sufficiently large set of biases, V_i, or at a reduced level of accuracy by deriving $\partial_z \partial_V I$ from two $\partial_V I$-V curves measured at different tip-sample separations.

For the sake of simplicity we presented the proposed formalism within the frame of the one-dimensional WKB approximation with the trapezoidal approximation of the transmission probability function. The formalism can easily be rewritten to include a general barrier potential, $W(z)$, e.g., a potential including the image potential. The general transmission probability according to the one-dimensional WKB approximation is given by $T=\exp(-B\int_{z_1}^{z_2} k dz)$ with k such that $\frac{\hbar^2 k^2}{2m_e} = W(z) - E$, and z_1 and z_2 are given by $V(z_i)=E$. Within the trapezoidal approximation $z_1=0$ and $z_2=d$ with the tip-sample separation, d. For a general potential, however, z_1 and z_2 may depend on W, E, V, and d. For better readability, we set the phase integral $P=\int_{z_1}^{z_2} k dz$. Then, Eq. (3) reads as

$$\partial_V I(V) = \rho_S(V)\rho_T(0)T(E=V,z) + \int_0^V \rho_S(E) T(E,V,z) \cdot [\partial_V \rho_T(E-V) - B\rho_T(E-V)\partial_V P] dE,$$

and Eq. (6) reads

$$\partial_z \partial_V I(V) = -B\rho_S(V)\rho_T(0)T(E=V,z) \cdot \partial_z P(E=V) + B \cdot \int_0^V \rho_S(E) T(E,V,z) [B \cdot \rho_T(E-V) \cdot \partial_z P \cdot \partial_V P - \rho_T(E-V) \cdot \partial_z \partial_V P - \cdot \partial_E \rho_T(E-V) \cdot \partial_z P] dE.$$

It is immediately clear that both formulas can be formally solved for $\rho_S(V)$ forming a Volterra integral equation of the second kind and, hence, the Neumann approximation scheme can be applied.

We now have two sets of integro-differential equations relating measurable data such as $I(V)$, $\partial_V I$, and $\partial_z \partial_V I$ to the solutions $\rho_S(E)$ and $\rho_T(E)$. The required parameters Φ and z may be determined experimentally from I-z curves or by a gentle touch, respectively, or by methods proposed in Refs. 8 and 12. Exploiting just one set of equations, e.g., Eqs. (4) and (5) at a given tip-sample separation, z_1, will always return a solution for one DOS depending on the initial choice of the second. However, applying this type of analysis effectively excludes exploitation of the separation dependence to obtain a possible deconvolution. As described above, it is the fundamental idea of the present contribution to take advantage of the additional information provided by the tip-sample separation dependence of the problem in order to optimize the solution path delivering deconvolution of the two unknown functions.[9] Referring to Eq. (2), this may be rephrased: without the transmission coefficient, $T(E,V,z)$, the integral is a simple convolution integral and deconvolution is in general impossible. $T(E,V,z)$, however, is neither symmetric in E, V, nor z and, therefore, its appearance under the integral lifts the symmetry of the equation making a deconvolution of ρ_S and ρ_T possible.

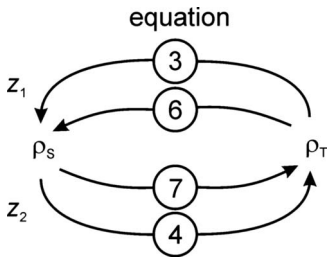

FIG. 2. Flow chart of optimizations. The arrows point to the function being optimized. An optimization typically includes several iterations.

III. APPLICATION OF THE NEUMANN APPROXIMATION SCHEME

In the following we want to analyze whether we are capable of deconvolving the DOS from given measurable data such as $I(V,z)$, $\partial_V I$, and $\partial_z \partial_V I$. So we will start our test with model functions for ρ_S and ρ_T and then calculate $I(V,z)$ from Eq. (1) for a preset set of voltages V_i. The derivatives are calculated numerically from $I(V_i,z)$ by calculating difference quotients. These calculated functions imitate experimental data and form the starting point of the deconvolution procedure. Since at first nothing shall be known about the functions ρ_S and ρ_T, it is reasonable to start with one function set to unity (here: $\rho_T=1$). According to the Neumann approximation scheme, the other function is set to zero (here: $\rho_S=0$). Figure 2 shows the flow chart for possible optimizations. The problem to be solved is then to find conditions and a path through the chart such that, at the end of the optimization, the resulting functions $\rho_{S,o}(E)$ and $\rho_{T,o}(E)$ solve self-consistently all equations.

We tried many combinations of pathways under the condition that both sets of equations are related to the same tip-sample separation, or say, the equations employed $\partial_V I(V,z_1)$ and $\partial_z \partial_V I(V,z_1)$, respectively. In all cases the deconvolution effect was unsatisfactory and the solutions diverged at least for one sign of the energy (consistently $\rho_{S,o}(E)$ and $\rho_{T,o}(E)$ at opposite signs). Apparently, for a given

tip-sample separation the information contained in the two functions $\partial_V I(V,z_1)$ and $\partial_z \partial_V I(V,z_1)$ is not sufficient to allow for an effective deconvolution of the DOS. Rather, numerical errors accumulate during the course of iteration. Consequently, we choose in the following, always two separations being sufficiently different, e.g., $z_1=2$ Å and $z_2=5$ Å. Note, that we will employ here both sets of Volterra equations. In the numerical examples given below this led to a fast convergence and, as a consequence, to a more accurate result. However, since consideration of the tunneling current and its derivatives at two different tip-sample separations always includes the full separation dependence, the optimization might also be successful if using just one set of equations but with two different separations. Section V will give an example of that.

According to our experience, the following scheme of optimization is typically successful: (i) iterate $\rho_{S,o}$ for $z_1 \leq z_2 - 2$ Å using Eq. (7) and $\rho_{T,o}=1$ until the relative change in subsequent iterations becomes small enough ($<10^{-6}$), (ii) iterate $\rho_{T,o}$ for z_2 using Eq. (8) accordingly, and (iii) cycle through (i) and (ii) six times. More cycles should be avoided since numerical errors accumulate showing up as diverging DOS at the boundaries. Note, that apparently the result of these calculations depends sensitively on numerical errors. The numerical errors being of interest here are not related to a limited precision of numbers. They are related to errors occurring when numerically differentiating and integrating discretized data. For typical tunneling conditions these errors will be amplified by each subsequent cycle by a factor of about ten.

IV. EXAMPLES

Figure 3 shows three examples of successful DOS recovery and deconvolution. In the first case, the initial DOS of the tip is unity and the DOS of the sample is unity with two additional Gaussian peaks at +0.6 and −1.2 eV. The Gaussian peaks have a width and an area of 0.3 eV corresponding to a height of about 0.8. After applying our scheme [Fig. 3(a)], the DOS of the sample is recovered at an accuracy of 0.01. The DOS of the tip is recovered similarly accurately in the energy range above −1.8 eV. However, below −1.8 eV the numerical errors accumulated and piled up to −0.5 at −2.5 eV. This example shows that the peaks positioned at both signs of the bias are recovered in the sample DOS and the DOS of the tip remains essentially unchanged.

For the second example [Fig. 3(b)], we choose a Gaussian peak at +0.6 eV in the sample DOS and a Gaussian peak at +1.2 eV for the tip DOS on an otherwise constant background of unity. In comparison to the first example, the $\partial_V I$ signal [c.f. Fig. 3(b) inset] would show similar peaks at positive and negative biases since the peak at positive energy in the tip DOS appears at a negative bias in $\partial_V I$. This shows that the proposed algorithm is able to transfer information to the tip DOS. After applying our scheme, the DOS of the sample is recovered at an accuracy of better than 0.03 over all the displayed energy ranges. At the peak related to the tip DOS the deviation is 0.025 and at the upper boundary the deviation is 0.03. The tip DOS is recovered at an accuracy of better than 0.01 for energies above −1.9 eV, which includes the peak in the original DOS. Below −1.9 eV the absolute deviation from the original DOS increases sharply to 0.7. Obviously, the number of cycles (six also in this example) did suffice to almost completely transfer the information re-

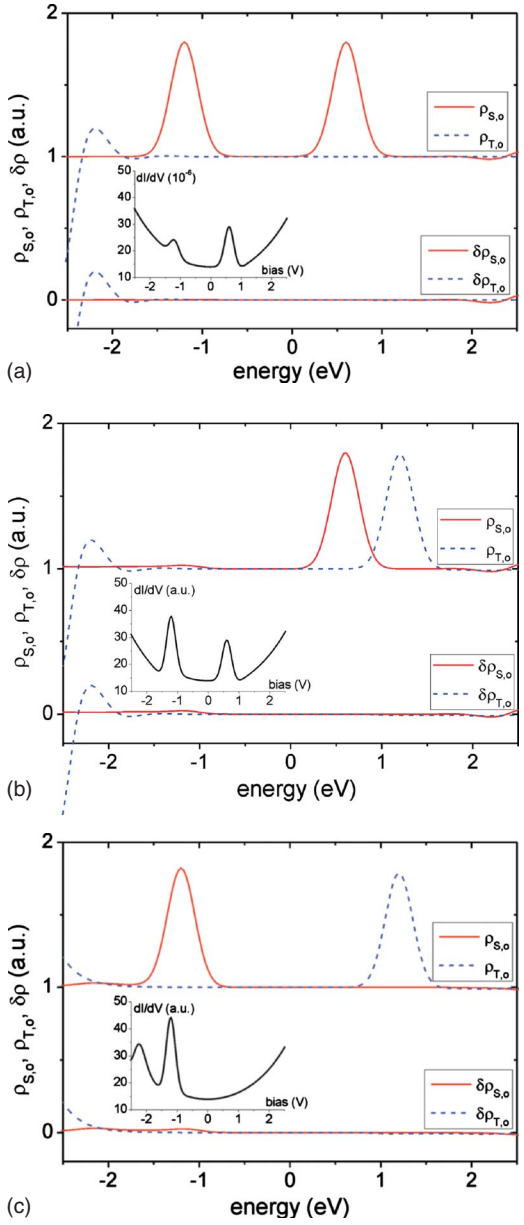

FIG. 3. (Color online) Recovered and deconvolved DOS together with the errors with respect to the original DOS [$\rho_{S,o}$ upper solid (red), $\rho_{T,o}$ upper dashed (blue), $\delta\rho_{S,o}$ lower solid (red), and $\delta\rho_{T,o}$ lower dashed (blue)] for different initial DOS: (a) $\rho_S=1$ with two Gaussian peaks at +0.6 and −1.2 eV, $\rho_T=1$, (b) $\rho_S=1$ with one Gaussian peak at +0.6 eV, $\rho_T=1$ with one Gaussian peak at +1.2 eV, and (c) $\rho_S=1$ with one Gaussian peak at −1.2 eV, $\rho_T=1$ with one Gaussian peak at +1.2 eV. In all cases we used two tip-sample separations $z_1=2$ Å and $z_2=5$ Å; the barrier height was $\Phi=5$ eV. We cycled the optimization of the DOS six times, and each optimization of a DOS was iterated ten times. The Gaussian peaks have a width and an area of 0.3 eV resulting in a height of about 0.8. The insets in the panels display $\partial_V I(V;z_2)$.

lated to the original tip DOS to the recovered tip DOS.

The third example [Fig. 3(c)] uses in both DOS a constant background of unity and one Gaussian peak at $E_{ps}=-1.2$ eV and $E_{pt}=+1.2$ eV in the sample and tip DOS, respectively. Both peaks show up in the $\partial_V I$ signal [c.f. Fig. 3(c) inset] at −1.2 V as a joint signature. In addition, however, there is a satellite at $E_{ps}-E_{pt}=-2.4$ eV.[12] After applying our scheme, the DOS of the sample is recovered at an accuracy of better than 0.03 all over the displayed energy range. The tip DOS is recovered at the same accuracy for energies above −2.1 eV and increases up to 0.23 at −2.5 eV. The average deviation from the original DOS, however, is still just 0.006.

These three examples clearly prove the principle of DOS recovery and deconvolution by the proposed algorithm within the framework of the one-dimensional WKB approximation. The algorithm is extendable to finite temperatures, and it could be applied as well to alternative transmission coefficients. However, the numerical errors encountered while treating the problem numerically as a whole point to difficulties when applying the formalism to experimental data being afflicted with noise, scaling errors, offsets, and drift effects. Nevertheless, such difficulties can be solved by, e.g., proper noise removal, self-consistency checks, and adjustment of the numerical scheme, as will be shown in the Sec. V.

V. APPLICATION TO EXPERIMENTAL DATA

With respect to fast convergence and high accuracy, the above-described formalism worked best, naturally, with numerical data. A more stringent test of the whole idea, however, is an application to experimental data like those obtained on Nb(110) Ref. 15) at low temperature. For this purpose, the following experimental procedure was performed. We measured a set of five separation-dependent $\partial_V I(V;z_j)$ curves by changing the set point of the initial tunneling current, i.e., we changed the tip-sample separation, z_j. Each $\partial_V I(V;z_j)$ curve comprises ~500 data points and represents the average over ten I-V scans. The error of such averages is typically 0.5%. Subsequently, we determined the tunneling barrier height, Φ, by acquiring an I-z scan at low bias. In the presented case we determined a barrier of (3.60 ± 0.01) eV. Though we do not know the actual tip-sample separation, we can determine a set of separation changes, $\Delta z_j=z_{j+1}-z_j$, such that $\partial_V I(V=0;z_j)=\partial_V I(V=0;z_{j+1})\times\exp(\sqrt{}\Phi\Delta z_j)$. This way we ensure that the different $\partial_V I(V;z_j)$ curves scale according to the WKB approximation at low bias, which is required for the formalism to work. Two of the scaled $\partial_V I(V;z_j)$ curves are displayed in Fig. 4(a). For comparison, we also calculated numerically the differential barrier height, $\partial_V\partial_z I(V;z_1)$, from the first two curves [inset in Fig. 4(a)]. The strong changes in $\partial_V\partial_z I(V;z_1)$ at positive bias indicate strong changes in the sample DOS at positive energy and/or the tip DOS at negative energy. The peak at −0.85 eV indicates a sudden drop of the sample DOS at that energy or the tip DOS at +0.85 eV [compare Eq. (6).

The deconvolution scheme is modified by employing Eq. (4) in step (i) instead of Eq. (7). We cycle just four times

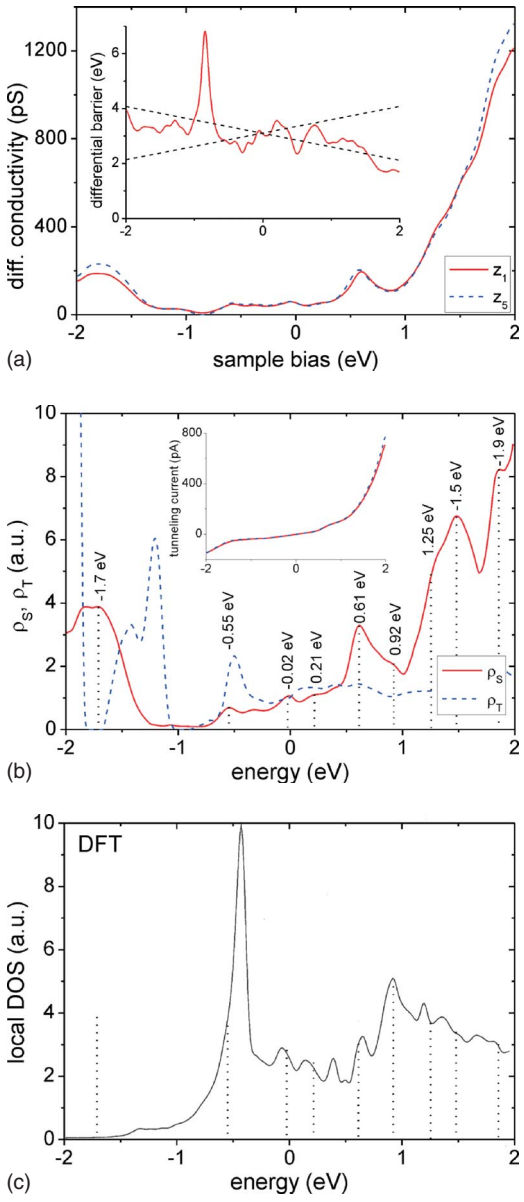

FIG. 4. (Color online) (a) Two scaled $\partial_V I(V;z_j)$ curves as described in the text using $\Delta z_j=0.113$ Å. The inset shows the differential barrier height, $\partial_V\partial_z I(V;z_1)$, calculated from $\partial_V I(V;z_1)$ and $\partial_V I(V;z_2)$. The dashed lines in the inset indicate the sample and tip barrier according to the trapezoidal approximation as introduced in Ref. 9. (b) The averaged deconvolved DOS of sample (solid) and tip (dashed). The inset shows the calculated tunneling current using the deconvolved DOS (dashed) together with the measured tunneling current (solid). (c) Density of electronic states 4 Å apart from the Nb(110) derived from DFT calculations. The dashed lines indicate the same signatures as in (b).

through the iteration scheme renouncing high precision thereby avoiding divergence at the interval boundaries, and we use a reasonable value for $z_1=4$ Å. In addition, we cut negative values of the DOS and set them to zero after each optimization of a DOS. We then apply the scheme pairwise to the experimental $\partial_V I(V;z_j)$ curves and average the resulting sample and tip DOS. The average DOS of the tip and the sample are displayed in Fig. 4(b). The error of the mean

value of the deconvolved sample DOS is typically 5% outside the gap ranging from −1.3 to −0.7 eV. Since the DOS is very small inside the gap, the error of the mean is up to 70% inside the gap. Note that the given error is related to the sample separation and gives us a hint to the stability of the solution. It does not include systematic errors due to, e.g., a restricted validity of the 1D WKB approximation. The inset in Fig. 4(b) displays the calculated tunneling current, $I(V;z_1)$, using the averaged DOS according to Eq. (2) along with the measured tunneling current. The excellent correspondence is obvious. A small deviation at positive bias is due to cutting the tip DOS at zero making the DOS physical.

The deconvolved tip DOS is relatively smooth at positive energies even though there is a strong peak in the differential barrier height at −0.9 eV [inset in Fig. 4(a)]. At negative energies, however, it varies strongly and tends to go negative left and right of the double peak at (−1.4,−1.2) eV. Varying z_1 in the range of 2–6 Å did not alter this tendency. It seems that this strong variation including (mathematically) negative values of the resulting tip DOS is required to shape the sample DOS at positive energies consistently with the 1D WKB approximation. This might be a hint that in that energy range the 1D WKB approximation is not sufficient to describe the tunneling between the Nb surface and the W tip accurately.

As expected from the differential barrier height [inset in Fig. 4(a)], the deconvolved sample DOS varies strongly for positive energy. Signatures noticeable in $\partial_V I$ as only a small peak or even as a shoulder appear strongly enhanced in the deconvolved sample DOS. The enhancement evolved step by step during each cycle of optimization and is moderated by cutting negative values of the tip DOS at negative energies. At negative energies, there is a broad pronounced peak at −1.7 eV and a gap between −1.3 and −0.7 eV. Within this gap there is a plateau ranging from −1.3 eV to −0.9 eV. It appears that the drop off at −0.9 eV caused the sharp peak in the differential conductivity.

We compare the deconvolved sample DOS to density-functional theory (DFT) calculations (full-potential linearized augmented plane-wave method, DFT theory applying local-density approximation, 19 layers, vertically unrelaxed, compare Ref. 16) of the vacuum density of electronic states 4 Å apart from the surface [Fig. 4(c)].[17] At energies above −0.6 eV, we find signatures in both curves at very similar energies, i.e., at [−0.45,−0.05,0.2,0.4,0.65,0.95,1.2, 1.4,1.7] eV in the DFT DOS and [−0.55,−0.05, 0.2,n.a.,0.65,0.95,1.3,1.5,1.85] eV in the deconvolved sample DOS. Evaluating just the positions of signatures, the similarity is striking. The relative amplitude of the signatures, however, is different in the DFT DOS and the deconvolved DOS. Though the relative amplitude of signatures may be influenced by changing the initial tip-sample separation, z_1, the deconvolved sample DOS showed in most cases a tendency to grow at positive energy while, apart from the increase at 0.6 eV, the DFT DOS is decreasing. Both DOS fall off sharply left of the peak at about −0.5 eV. The strong peak in the deconvolved sample DOS at −1.7 eV is not present in the DFT DOS. The origin of this peak is possibly a surface state, which is missing in the presented DFT calculation.[18]

VI. CONCLUSION

In summary, we introduced a formalism which enables recovery and deconvolution of the DOS of tip and sample from measurable quantities, i.e., from I, $\partial_V I$, and $\partial_z \partial_V I$. The proposed formalism appears to work reliably if data are taken for two sufficiently different tip-sample separations z_1 and z_2, e.g., $z_1=2$ Å and $z_2=5$ Å for our numerical examples. We applied an adapted formalism to experimental data measured on Nb(110) and find a reasonable correspondence of the deconvolved sample DOS to density-functional theory calculations of the vacuum DOS. Finally, we would like to mention that this formalism holds generally within the 1D WKB approximation and, thus, it may also be applied to tunneling systems involving organic molecules.

ACKNOWLEDGMENTS

We thank O. Marti, S. Bobaru, and A. Tschetschetkin for helpful discussions and the Deutsche Forschungsgemeinschaft for financial support under Grant No. SFB569. S. Heinze (University of Hamburg) provided the DFT data.

[1] J. G. Simmons, J. Appl. Phys. **34**, 1793 (1963).
[2] J. G. Simmons, J. Appl. Phys. **35**, 2655 (1964).
[3] C. B. Duke, *Tunneling in Solids* (Academic, New York, 1969).
[4] J. A. Stroscio, R. M. Feenstra, and A. P. Fein, Phys. Rev. Lett. **57**, 2579 (1986).
[5] J. A. Stroscio and R. M. Feenstra, in *Methods of Experimental Physics*, edited by J. A. Stroscio and W. J. Kaiser (Academic, New York, 1993), Vol. 27.
[6] P. Mårtensson and R. M. Feenstra, Phys. Rev. B **39**, 7744 (1989).
[7] R. M. Feenstra, Phys. Rev. B **50**, 4561 (1994).
[8] V. A. Ukraintsev, Phys. Rev. B **53**, 11176 (1996).
[9] B. Koslowski, C. Dietrich, A. Tschetschetkin, and P. Ziemann, Phys. Rev. B **75**, 035421 (2007).
[10] C. Wagner, R. Franke, and T. Fritz, Phys. Rev. B **75**, 235432 (2007).
[11] M. Passoni and C. E. Bottani, Phys. Rev. B **76**, 115404 (2007).
[12] M. Passoni, F. Donati, A. Li Bassi, C. S. Casari, and C. E. Bottani, Phys. Rev. B **79**, 045404 (2009).
[13] P. Wahl, L. Diekhöner, M. A. Schneider, and K. Kern, Rev. Sci. Instrum. **79**, 043104 (2008).
[14] T. E. Feuchtwang, P. H. Cutler, and N. M. Miskovsky, Phys. Lett. A **99**, 167 (1983).
[15] B. Koslowski, C. Dietrich, and P. Ziemann, Surf. Sci. **557**, 255 (2004).
[16] M. Bode, S. Krause, L. Berbil-Bautista, S. Heinze, and R. Wiesendanger, Surf. Sci. **601**, 3308 (2007).
[17] S. Heinze (unpublished).
[18] Ch. E. Lekka, M. J. Mehl, N. Bernstein, and D. A. Papaconstantopoulos, Phys. Rev. B **68**, 035422 (2003).